Analytical mass transfer coefficients for natural convection from vertical gas-evolving electrodes

Valle, N.; Haverkort, J. W.

DOI
10.1016/j.ijheatmasstransfer.2024.125390

Publication date
2024

Document Version
Final published version

Published in
International Journal of Heat and Mass Transfer

Citation (APA)
Valle, N., & Haverkort, J. W. (2024). Analytical mass transfer coefficients for natural convection from vertical gas-evolving electrodes. *International Journal of Heat and Mass Transfer*, *225*, Article 125390. https://doi.org/10.1016/j.ijheatmasstransfer.2024.125390

International Journal of Heat and Mass Transfer 225 (2024) 125390

Contents lists available at ScienceDirect

International Journal of Heat and Mass Transfer

journal homepage: www.elsevier.com/locate/ijhmt

Analytical mass transfer coefficients for natural convection from vertical gas-evolving electrodes

N. Valle *, J.W. Haverkort

Process & Energy Department, Delft University of Technology, Leegwaterstraat 39, 2628 CB, Delft, the Netherlands

A B S T R A C T

The high mass transfer to or from gas-evolving electrodes is an attractive feature of electrochemical reactors, which can be partly attributed to the large convective flows that arise due to the buoyancy of bubbles. We derive exact analytical expressions for mass transfer coefficients for the case of constant gas flux boundary conditions. For the mass transport both Dirichlet and Neumann boundary conditions are considered. We deploy a recently derived self-similar solution of laminar two-phase flows, with density, hydrodynamic diffusivity, and viscosity dependent on the local gas fraction. Combining this with the Lévêque approximation, new mass transfer coefficients are obtained analytically. These new results are relevant for various electrochemical processes with gas evolution as well as boiling. The new formulation shows the mass transfer coefficient to scale with the vertical coordinate z proportional to $z^{-1/5}$ for short electrodes and low current densities and $z^{-4/15}$ for long ones and high current densities. The former limit also applies when buoyancy is due to temperature or concentration differences in the case that density differences are small. We provide a general overview considering all possible gas and mass boundary conditions combinations and a comparison with the Boussinesq approximation of small density differences.

1. Introduction

Mass transfer to or from a gas-evolving vertical plate is a phenomenon of paramount industrial relevance, for example, to water electrolysis [1–3], the synthesis of chlorine, sodium hydroxide [4], sodium chlorate [5] or aluminium [6]. Such multiphase flow systems benefit from the inexpensive stirring produced by buoyant bubbles, which set the fluid in a convective motion, improving the mass transfer of dissolved species in the liquid phase and thus shifting the reaction forward by removing products from the electrode. Mass transfer plays an essential role in the design, operation and safety of electrochemical reactors. For example, in water electrolysis, the concentration of dissolved species at the electrode determines gas crossover, which can lead to an explosive mixture. Therefore, poor mass transfer can restrict the safe operating regime of the electrolyser. Describing the mass transfer coefficients of dissolved species near gas-evolving electrodes then becomes increasingly relevant for the energy transition, in which electrochemical processes have an essential role to play.

The two-phase flow system under study comprises a liquid-gas mixture, which we model as a single fluid [7]. We assume that bubbles disperse similarly to the diffusion of temperature, as has been observed also for solid particles [8]. At very low gas fractions, the Boussinesq approximation holds for the mixture and we can assume a constant mixture density equal to that of the liquid, except for the buoyancy force. Under these conditions, two-phase, buoyant systems become analogous to thermally buoyant ones. For laminar flows, self-similarity solutions are well known [9–11], and have been extended, for example, to inclined plates [12,13]. For a complete review of laminar solutions using the Boussinesq approximation, the reader is referred to [14] and references therein. Nonetheless, the usual Boussinesq approximation is not valid in general, owing to the strong influence of gas fraction on density and viscosity, and the relatively high gas fraction present in two-phase flow reactors. Actually, results considering variable physical properties are largely absent in the literature. However, we recently obtained a self-similarity solution for laminar bubbly flows developing along a gas-evolving plate [15]. This analytical solution will be used in this paper to obtain general expressions for mass transfer coefficients.

Because the mass diffusivity (D) is usually much smaller than the kinematic viscosity (ν) we can use the Lévêque approximation, which assumes that the mass transfer boundary layer is much thinner than the hydrodynamic one, and thus the velocity profile can be linearised. Early publications applied such approximation to mass transfer in forced laminar [16–18] and turbulent [19–21] flows. Free thermal convection studies [22–24] also kept such an approximation, together with the Boussinesq approximation. These results were extended to general Schmidt numbers [25,26], including aiding and opposing buoyancy forces.

* Corresponding author.
E-mail addresses: n.vallemarchante@tudelft.nl (N. Valle), j.w.haverkort@tudelft.nl (J.W. Haverkort).

https://doi.org/10.1016/j.ijheatmasstransfer.2024.125390
Received 10 November 2023; Received in revised form 6 February 2024; Accepted 26 February 2024
Available online 8 March 2024

Nomenclature

$\mathcal{V}_m$	Molar volume	m^3/mol
c	Molar concentration	mol/m^3
D	Mass diffusivity	m^2/s
D_b	Bubble diffusivity	m^2/s
d_b	Bubble diameter	m
f_g	Gas evolution efficiency	
j	Current density	A/m^2
k	Mass transfer coefficient	m/s
N	Mass flow rate	$mol/m^2/s$
n_c	Number of molecules per electron	
u	Horizontal liquid velocity	m/s
U_w	Gas flux at the wall/electrode	m/s
w	Vertical liquid velocity	m/s
x	Horizontal coordinate	m
z	Vertical coordinate	m
H	Height of the electrode	m
w'	Vertical shear strain	1/s

Constants

F	Faraday's constant 96485.332...	C/mol
R	Gas constant 8.31446...	J/mol/K

Dimensionless numbers

Ar_{*z}	Local modified Archimedes number $\frac{gU_w z^4}{\nu^2 D_b}$
Pe_{bz}	Local bubble Péclet number $U_w z/D_b$
Sc	Schmidt number ν/D.
Sh_z	Local Sherwood number kz/D.

Greek variables

ν	Liquid's kinematic viscosity	m^2/s
ε	Void fraction	
δ_c	Mass transfer boundary layer thickness	m
δ_g	Gas plume thickness	m

Subscripts and other notation

B	Boussinesq
D	Dirichlet
N	Neumann

Most papers on natural convection considering heat and mass transfer deal with Dirichlet boundary conditions both for wall temperature and concentration, while only a few articles deal with Neumann boundary conditions of constant heat and/or mass flux. This can be attributed to no similarity transformation being possible for the general case [27,28]. For natural thermal convection, using Neumann boundary conditions does not result in a substantial difference compared with the Dirichlet case [10], which may partially explain why most attention goes to the slightly simpler use of Dirichlet boundary conditions.

However, the gas fraction at the wall is usually far from constant in gas-evolving electrodes. In contrast, the assumption of constant gas flux, associated with a constant current density, is often a good one-for reactions in which charge transfer is the rate-determining step. This is usually the case in which the products are easily removed from the reactive sites, and reactants are abundant, like in water electrolysis. By neglecting solutal buoyancy and using the Lévêque approximation, we can obtain self-similar solutions for both types of solutal boundary conditions [29]. Previous works that included solutal Neumann boundary conditions considered only linearised Poiseuille flows [27,29–31]. Therefore, we will extend previous results in the literature to apply to buoyant two-phase flows with constant gas evolution. To our knowledge, the present paper is the first approach to a self-similar solution of natural convection with variable physical properties, with constant gas evolution and considering both Neumann and Dirichlet boundary conditions for mass transfer.

Beyond the classical convective mass transfer mechanism, an additional stirring due to bubbles departing from, sliding along and/or coalescing on the electrodes, sometimes called micromixing, often dominates [32,33]. This is not always the case. For example, hydrogen bubbles in alkaline electrolytes show very little micromixing [34] so that mass transfer is dominated by macroscopic convection. Here, we limit ourselves to studying the background mass transfer coefficient, without micromixing.

2. Model

Mass transfer boundary layers δ_c are thin compared to the momentum boundary layer, since usually $\nu \gg D$ by several orders of magnitude. Therefore, when solving for mass transfer one can linearise the velocity in the vicinity of the wall as $w(x,z) \approx w'(z)x$. This is known as the Lévêque approximation [29] of the mass conservation equation (see Fig. 1), which in terms of molar concentration c reads:

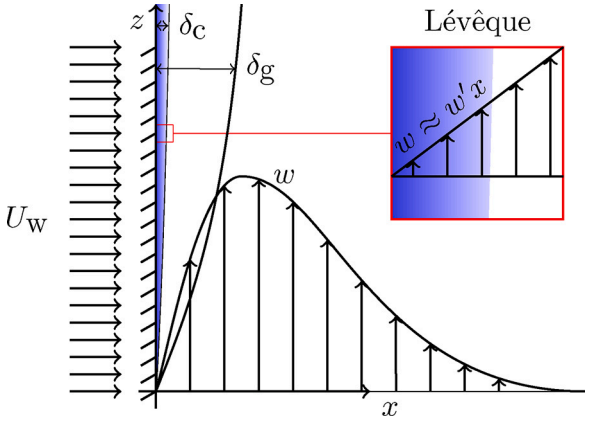

Fig. 1. Schematic of a gas-evolving vertical electrode. Mass δ_c and momentum boundary layers develop along the plate, together with a gas plume δ_g. When the mass transfer boundary layer δ_c is very thin compared with the momentum boundary layer, the mass transfer boundary layer can be linearised.

$$w' x \frac{\partial c}{\partial z} = D \frac{\partial^2 c}{\partial x^2} \tag{1}$$

where we have neglected streamwise diffusion, according to boundary layer theory. The Dirichlet boundary condition

$$c|_w = c_w \qquad \lim_{x\to\infty} c = c_\infty \tag{2a}$$

is often the most relevant one. Here $c_w = 0$ is a good approximation for mass transfer experiments in which a very reactive species is used so that its concentration vanishes at the wall. It may alternatively be replaced with the Neumann condition

$$D \left.\frac{\partial c}{\partial x}\right|_w = N \qquad \lim_{x\to\infty} c = c_\infty \tag{2b}$$

with $N > 0$ the constant flux of a reactant with concentration c or, in case $N < 0$, the flux of a product with concentration c. If the mass transfer is considered of a species that is involved in an electrochemical reaction, we have $N = \pm(1 - f_g)j/n_c F$ with f_g the gas evolution efficiency [35] (i.e., the fraction of moles that leave the electrode in gas form over the total electrochemical production), j the current density, n_c the number of electrons transferred per molecule of reactant/product whose concentration is c.

Note that the influence of flow in mass transport is introduced through the shear strain w' which, neglecting solutal buoyancy, is independent of c. Focusing on laminar flows developing along vertical gas-evolving electrodes, we will obtain w' from recent results [15], which consider variable density, viscosity and diffusivity.

For gas-evolving electrodes, the volumetric flux of gas can be related to the current density by Faraday's law [35,36].

$$U_\mathrm{w} = f_g \frac{j\mathcal{V}_\mathrm{m}}{n_c F} \tag{3}$$

where the molar volume is given for an ideal gas by $\mathcal{V}_\mathrm{m} = RT/p$ and n_c is the number of electrons transferred per gas molecule produced.

The mass conservation equation (1) allows a simple self-similar solution for both Dirichlet and Neumann cases when D/w' is constant or only a function of z [29]. Here, we will sketch only the essential steps and the results, whereas their complete derivations are provided in Appendix A. We will introduce the following self-similar variable

$$\xi \equiv \frac{x}{L_z} \tag{4}$$

where the characteristic length is

$$L_z = \left(9\int_0^z \frac{D}{w'}\,dz\right)^{1/3} \tag{5}$$

This transformation converts equation (1) into an ODE, which can be solved analytically in terms of ξ only. Fig. A.4 shows the solution of the dimensionless concentration profiles in terms of ξ for both Neumann and Dirichlet boundary conditions. Note that the flow profile only enters through w' in the definition of L_z. From the analytical solution in Appendix A.1, we obtain the mass transfer coefficient

$$k_D \equiv \frac{D}{c_\mathrm{w} - c_\infty}\left.\frac{\partial c}{\partial x}\right|_\mathrm{w} \approx 1.12\frac{D}{L_z} \tag{6}$$

Defining a local Sherwood number $\mathrm{Sh}_{\mathrm{D,z}} \equiv k_D z/D$ we see that $\mathrm{Sh}_{\mathrm{D,z}} \approx 1.12 z/L_z$.

The mass transfer coefficient for the Neumann case k_N is obtained assuming that not the wall concentration but the flux of species is constant as in equation (2b). The resulting expression, derived in Appendix A.2, is identical to the Dirichlet case except for a slightly different prefactor

$$\frac{k_\mathrm{D}}{k_\mathrm{N}} \approx 0.827 \tag{7}$$

For this reason, and to lighten the exposition, we will only present the results for the case of k_D, from which k_N can be easily obtained.

3. Results

To be able to evaluate equation (6) for the mass transfer coefficient, we have to evaluate L_z which depends on the shear strain at the wall, w'. For bubbly flows developing along a vertical electrode, we will use [15]

$$w' \approx (1-\varepsilon_\mathrm{w})\left(\frac{g^3 U_\mathrm{w}^3 z^2}{\nu D_\mathrm{b}^3}\right)^{1/5} f''_\mathrm{w} \tag{8}$$

Bubbles' diffusivity is defined as:

$$D_\mathrm{b} = \frac{g d_\mathrm{b}^3}{36\nu} \tag{9}$$

This relation was determined for settling solid particles and is assumed to hold equally for non-coalescing bubbles [37,38]. The prefactor, featuring the wall gas fraction ε_w, reads

$$1-\varepsilon_\mathrm{w} = \frac{1}{1+\left(\frac{\nu^2 U_\mathrm{w}^4 z}{g D_\mathrm{b}^4}\right)^{1/5}\theta_\mathrm{w}} \tag{10}$$

where [15][1]:

$$\theta_\mathrm{w} \approx \begin{cases} 1.63\mathrm{Pr}_\mathrm{b}^{-9/25} & \mathrm{Pr}_\mathrm{b} \geq 1 \\ 1.63\mathrm{Pr}_\mathrm{b}^{-1/5} & \mathrm{Pr}_\mathrm{b} \leq 1 \end{cases} \tag{13}$$

$$f''_\mathrm{w} \approx \begin{cases} 1.5\mathrm{Pr}_\mathrm{b}^{-2/5} & \mathrm{Pr}_\mathrm{b} \geq 1 \\ 1.5\mathrm{Pr}_\mathrm{b}^{-1/3} & \mathrm{Pr}_\mathrm{b} \leq 1 \end{cases} \tag{14}$$

where the bubble Prandtl number is defined as

$$\mathrm{Pr}_\mathrm{b} \equiv \frac{\nu}{D_\mathrm{b}} \approx \frac{18\nu^2}{g d_\mathrm{b}^2} \tag{15}$$

With $\nu = 10^{-6}$ m^2/s and $d_\mathrm{b} = 100$ μm this gives $\mathrm{Pr}_\mathrm{b} \approx 1$ so that for typical aqueous electrolytes the conditions $\mathrm{Pr}_\mathrm{b} > 1$ and $\mathrm{Pr}_\mathrm{b} < 1$ translate, approximately, to the limits $d_\mathrm{b} < 100$ μm and $d_\mathrm{b} > 100$ μm, respectively.

For very small heights and gas fluxes, the denominator in equation (10) is close to one so the wall gas fraction $1-\varepsilon_\mathrm{w}$ is small and the shear rate scales with $z^{2/5}$. For larger heights and gas fluxes, the denominator can be much larger than one so the wall tends to one, in which case the shear rate becomes proportional to $z^{1/5}$.

Next, we determine the characteristic length L_z from equation (5) by inserting equations (8) and (10) and integrating to give

$$L_z = \left(\frac{D_\mathrm{b} z}{g U_\mathrm{w}}\right)^{\frac{1}{5}}\left(\frac{15 D \nu^{\frac{1}{5}}}{f''_\mathrm{w}}\left(1+\frac{3\theta_\mathrm{w}}{4}\left(\frac{\nu^2 U_\mathrm{w}^4 z}{g D_\mathrm{b}^4}\right)^{\frac{1}{5}}\right)\right)^{\frac{1}{3}} \tag{16}$$

from which we can immediately obtain the mass transfer coefficient $k_D \approx 1.12 D/L_z$ as

$$k_\mathrm{D} \approx \frac{0.454 D^{2/3}(f''_\mathrm{w})^{1/3}\left(\frac{g U_\mathrm{w}}{\nu^{1/3} D_\mathrm{b} z}\right)^{1/5}}{\left(1+\frac{3}{4}\theta_\mathrm{w}\left(\frac{\nu^2 U_\mathrm{w}^4 z}{g D_\mathrm{b}^4}\right)^{1/5}\right)^{1/3}} \tag{17}$$

This shows a transition from a scaling with $z^{-1/5}$ to $z^{-4/15}$. These two asymptotes are equal for $z = z_\mathrm{c}$ where

$$z_\mathrm{c} = \left(\frac{4}{3\theta_\mathrm{w}}\right)^5 \frac{g D_\mathrm{b}^4}{\nu^2 U_\mathrm{w}^4}. \tag{18}$$

We do note that because of the very low power of $z^{1/5}$, the transition region is smeared out over a very wide range of heights, and in practice, neither of the limits will be easily attainable. In terms of current density, there is a transition from scaling with $U_\mathrm{w}^{1/5}$ to $U_\mathrm{w}^{-1/15}$ so that beyond a certain gas flux, the mass transfer coefficient decreases with increasing gas flux. The gas flux for which the mass transfer is optimal is given by

$$U_\mathrm{w,opt} = 4 D_\mathrm{b}\left(\frac{g}{\theta_\mathrm{w}^5 \nu^2 z}\right)^{1/4} \tag{19}$$

which will usually only be achieved at very high current densities. In dimensionless notation equation (17) reads for the Sherwood number $\mathrm{Sh}_{\mathrm{D,z}} = k_D z/D$:

[1] Approximations valid for all Pr_b are given by

$$\theta_\mathrm{w} \approx 1.63\left(\mathrm{Pr}_\mathrm{b}^{-9/5} + \mathrm{Pr}_\mathrm{b}^{-1}\right)^{1/5} \tag{11}$$

$$f''_\mathrm{w} \approx 1.5\left(\mathrm{Pr}_\mathrm{b}^{-6} + \mathrm{Pr}_\mathrm{b}^{-5}\right)^{1/15} \tag{12}$$

These give maximum relative errors of roughly 3% and 5%, respectively.

$$\mathrm{Sh}_{\mathrm{D},z} \approx 0.454 \left(\frac{\mathrm{Sc} f''_{\mathrm{w}} \mathrm{Ar}_{*z}^{3/5}}{1 + \frac{3}{4}\theta_{\mathrm{w}} \mathrm{Pe}_{\mathrm{b}z} \mathrm{Ar}_{*z}^{-1/5}} \right)^{1/3} \tag{20}$$

In the limit $\mathrm{Pr}_{\mathrm{b}} \geq 1$, typically for small bubbles with $d_{\mathrm{b}} \lesssim 100$ μm, equations (17), (13), and (14) give

$$k_{\mathrm{D}} \approx \frac{0.52 D^{2/3} \left(\frac{g U_{\mathrm{w}}}{\nu D_{\mathrm{b}}^{1/3} z} \right)^{1/5}}{\left(1 + 1.2 \left(\frac{\nu U_{\mathrm{w}}^4 z}{g D_{\mathrm{b}}^3} \right)^{1/5} \right)^{1/3}} \tag{21}$$

In the limit $\mathrm{Pr}_{\mathrm{b}} < 1$, typically for relatively large bubbles with $d_{\mathrm{b}} \gtrsim 100$ μm, equations (17), (13), and (14) give

$$k_{\mathrm{D}} \approx \frac{0.52 D^{2/3} \left(\frac{g U_{\mathrm{w}} D_{\mathrm{b}}^{2/3}}{\nu^2 z} \right)^{1/5}}{\left(1 + 1.2 \left(\frac{\nu^{1/3} U_{\mathrm{w}}^4 z}{g D_{\mathrm{b}}^{7/3}} \right)^{1/5} \right)^{1/3}} \tag{22}$$

In case of low heights and low gas flux the denominator of equations (17) or (20) approaches one, which agrees with the classical result of natural thermal convection [10] that is obtained using the Boussinesq approximation. In this limit, the gas fraction is so small that its effect on density, viscosity, and hydrodynamic dispersion is negligible. Our new solution is more general as it includes the effect of a finite gas fraction on inertia, bubble dispersion, and viscosity. In the somewhat artificial opposite limit of $\varepsilon_{\mathrm{w}} \to 1$, the denominator is much larger than one, the wall gas fraction tends to one and both the effective viscosity and hydrodynamic dispersion coefficients diverge. Because of the uncertainty in the dependencies of viscosity and bubble dispersion coefficient on gas fraction, the possible relevance of other bubble forces, and the possible occurrence of turbulence, the experimental relevance of this limit remains to be seen.

Note that in the limit of unit wall gas fraction, the mass transfer coefficient no longer depends on the bubble dispersion coefficient for small bubbles. Also, the dependence on gas flux becomes extremely small, while the dependence on height increases compared to that at low to moderate gas fractions.

Our new formulation can be compared with the Boussinesq approximation, $k_{\mathrm{D,B}}$, which follows from setting the denominator of equation (17) to 1. After isolating the $\theta_{\mathrm{w}} \left(\frac{\nu^2 U_{\mathrm{w}}^4 z}{g D_{\mathrm{b}}^4} \right)^{1/5}$ group from equation (10), the ratio between the two reads:

$$\frac{k_{\mathrm{D}}}{k_{\mathrm{D,B}}} = \left(1 + \frac{3}{4} \frac{\varepsilon_{\mathrm{w}}}{1 - \varepsilon_{\mathrm{w}}} \right)^{-1/3} \tag{23}$$

As can be seen in Fig. 2, this typically gives modest corrections except for very high gas void fractions, in which case the mass transfer coefficient dramatically decreases.

The new expression for mass transfer coefficient is plotted against experimental data taken from [39] in Fig. 3. Physical properties were taken from [40]. These works used a pair of marker ions in the electrolyte solution which react rapidly at the electrode, resulting in an effective Dirichlet boundary condition for the concentration at the electrodes. We focus on the cathode, which evolves H_2 bubbles and whose diameter is typically $d_{\mathrm{b}} \approx 50$ μm [34], so equation (21) is the most relevant for this case. The height-averaged mass transfer coefficient $\langle k_{\mathrm{D}} \rangle$, relative to the local mass transfer coefficient k_{D} can be obtained from Eq. (17) by integration as

$$\frac{\langle k_{\mathrm{D}} \rangle}{k_{\mathrm{D}}} = \frac{243}{88 \bar{z}^{\frac{4}{5}}} \left(\left(1 + \bar{z}^{\frac{1}{5}} \right)^{\frac{1}{3}} - 1 - \frac{1}{3}\bar{z}^{\frac{1}{5}} + \frac{1}{9}\bar{z}^{\frac{2}{5}} - \frac{5}{81}\bar{z}^{\frac{3}{5}} + \frac{40}{81}\bar{z}^{\frac{4}{5}} \right) \tag{24}$$

where $\bar{z} \equiv z/z_{\mathrm{c}}$. This tends between the two limits of $5/4 = 1.25$ for $\bar{z} \to 0$ and $15/11 \approx 1.36$ for $\bar{z} \to \infty$. For $\bar{z} = 1$ we obtain $\langle k_{\mathrm{D}} \rangle / k_{\mathrm{D}} \approx 1.3$, which has less than 5% difference with either limits. Therefore, we can reasonably accurately obtain the height-average mass transfer coefficient by simply multiplying the mass transfer coefficient at the top by 1.3, which is what we did in Fig. 3.

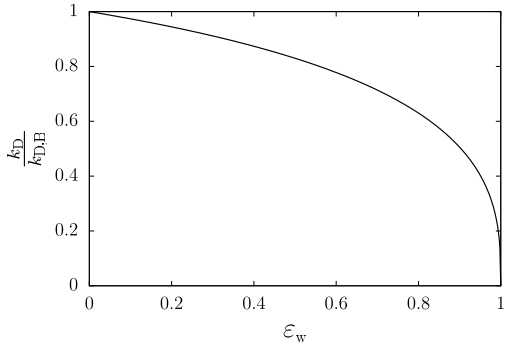

Fig. 2. The correction factor of equation (23) comparing the new result *versus* the mass transfer coefficient obtained from the classical Boussinesq approximation valid for low gas fractions.

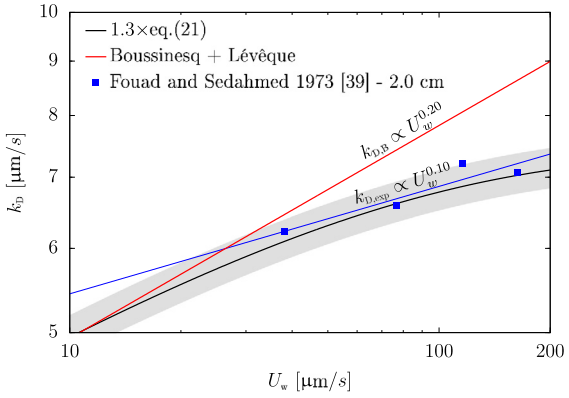

Fig. 3. Average mass transfer coefficients in a H_2-evolving system for our new model compared with the Boussinesq approximation and experimental data taken from [39]. The setup consists of a $H = 10$ cm height electrode immersed into a 2M NaOH electrolyte with 0.1M $K_3(CN)_6$ and 0.1M $K_4(CN)_6$. A typical bubble diameter $d_{\mathrm{b}} \approx 50$ μm is assumed. The band between the lower and upper limits of the average mass transfer coefficient (corresponding to $5/4 \times$ eq. (21) for $\bar{z} \to 0$ and $15/11 \times$ eq. (21) for $\bar{z} \to \infty$) is shown in grey. (For interpretation of the colours in the figure(s), the reader is referred to the web version of this article.)

Results show an excellent agreement with the data from [39] for $d_{\mathrm{b}} = 50$ μm. The scaling of the experimental results is approximately $\sim z^{0.1}$, which is captured with the new model, whereas the classical Boussinesq theory predicts $\sim z^{0.2}$ The results do not sensitively depend on d_{b} in the range between $20 - 80$ μm, whereas the sensitivity to mass diffusion coefficient is much higher.

4. Conclusions

We obtained combined similarity solutions for natural convection and mass transfer by using the Lévêque approximation and boundary layer theory. The used self-similarity solution [15] takes into account the effect of gas fraction on density, mixture viscosity and bubble hydrodynamic dispersion.

We have considered Neumann boundary conditions, often most relevant for electrochemical processes, for the gas fraction and Dirichlet or Neumann conditions for the concentration. We show that the difference between Dirichlet and Neumann boundary conditions for concentration is a simple numerical factor. That is, the mass transport coefficient of a non-buoyant species with Dirichlet boundary conditions is

$3\sqrt{3}/2\pi \approx 0.827$ times that in the case of Neumann boundary conditions.

The new mass transfer coefficient shows a mixed scaling with height z, asymptotically transitioning from a proportionality with $z^{-1/5}$ to $z^{-4/15}$ as the wall gas fraction tends to one. We report our new results along with the classical Boussinesq result, where the latter is shown to hold for low wall gas fractions. The comparison shows a moderate correction compared to the low wall gas fraction result, which becomes very large at very high wall gas fractions.

Experimental results from the literature are in excellent agreement with the model, and most remarkably capture the right shape of the experimental results.

CRediT authorship contribution statement

N. Valle: Conceptualization, Formal analysis, Investigation, Methodology, Validation, Writing – original draft, Writing – review & editing. **J.W. Haverkort:** Conceptualization, Funding acquisition, Investigation, Methodology, Project administration, Supervision, Validation, Writing – review & editing.

Declaration of competing interest

The authors declare that they have no known competing financial interests or personal relationships that could have appeared to influence the work reported in this paper.

Data availability

No data was used for the research described in the article.

Acknowledgements

We acknowledge the Dutch Research Council (NWO) for funding under grant agreement KICH1.ED04.20.011.

Appendix A. Lévêque approximation

The similarity solution of equation (1) in the case of Dirichlet boundary conditions can be found in many textbooks and papers on heat transfer [22,29,30]. However, the solution for Neumann boundary conditions is not often encountered. In [29], a solution is provided in the context of a laminar flow through a tube with constant heat flux by transforming the flux as a new primitive variable. Here, we will follow another strategy: changing the self-similarity prototype function to match the Neumann boundary conditions and then solving the resulting self-similar equation analytically.

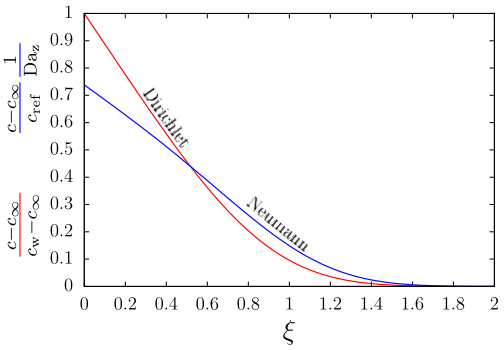

Fig. A.4. Mass transfer profile for Dirichlet and Neumann boundary conditions at the electrode.

A.1. Dirichlet

The similarity variable ξ of equation (4) transforms equation (1) and the boundary conditions (2), into

$$c'' + 3\xi^2 c' = 0 \tag{A.1}$$

$$c(0) = c_\mathrm{w} \qquad \lim_{\xi\to\infty} c = c_\infty \tag{A.2}$$

The solution reads

$$\frac{c - c_\infty}{c_\mathrm{w} - c_\infty} = \mathrm{Q}\left(\frac{1}{3}, \xi^3\right) \tag{A.3}$$

where Q is the regularized upper incomplete gamma function $\mathrm{Q}(1/3,\xi^3) = \Gamma(1/3,\xi^3)/\Gamma(1/3)$, where $\Gamma(1/3,\xi^3) = \int_{\xi^3}^{\infty} t^{-2/3}\mathrm{e}^{-t}dt$ and $\Gamma(1/3) = \Gamma(1/3,0) \approx 2.67894$. With a single argument, $\Gamma(x)$ is called the gamma function without another descriptor.

The concentration gradient at the wall $\left.\frac{\partial c}{\partial x}\right|_\mathrm{w} = \lim_{x\to 0^+}\frac{\partial c}{\partial x}$ is:

$$\left.\frac{\partial c}{\partial x}\right|_\mathrm{w} = -\frac{3\left(c_\mathrm{w} - c_\infty\right)}{\Gamma\left(\frac{1}{3}\right) L_z} \tag{A.4}$$

where $3/\Gamma(1/3) \approx 1.1198$.

This gives the mass transfer coefficient $k = \frac{D}{c_\infty - c_\mathrm{w}}\left.\frac{\partial c}{\partial x}\right|_\mathrm{w}$ as

$$k = \frac{3}{\Gamma(1/3)}\frac{D}{L_z} \approx 1.1198\frac{D}{L_z} \tag{A.5}$$

In dimensionless form, we define the dimensionless concentration with $c_\mathrm{ref} = c_\mathrm{w} - c_\infty$ so $\bar{c} = (c - c_\infty)/\left(c_\mathrm{w} - c_\infty\right)$ and

$$\bar{c} = \mathrm{Q}\left(\frac{1}{3}, \xi^3\right) \tag{A.6}$$

The dimensionless wall concentration gradient:

$$\left.\frac{\partial \bar{c}}{\partial x}\right|_\mathrm{w} = \frac{3}{\Gamma\left(\frac{1}{3}\right) L_z} \tag{A.7}$$

Finally, the local Sherwood number reads:

$$\mathrm{Sh}_z = \frac{3}{\Gamma\left(\frac{1}{3}\right)}\frac{z}{L_z} \approx 1.1198\frac{z}{L_z} \tag{A.8}$$

The mass transfer boundary layer thickness is defined to be the length from the wall at which the concentration decreases to 0.01 at $\xi = 1.4037$ so that the 99% concentration boundary layer thickness is given by $\delta_{99\%} = 1.4037 L_z$.

A.2. Neumann

Together with the coordinate transformation stated in equation (4), we attempt solutions of the following form:

$$c - c_\infty = \hat{c}(\xi) L_z \tag{A.9}$$

to transform equation (1) and the boundary conditions (2) into:

$$\hat{c}'' + 3\xi^2\hat{c}' - 3\xi\hat{c} = 0 \tag{A.10}$$

$$\hat{c}'(0) = \frac{j}{nFD} \qquad \lim_{\xi\to\infty}\hat{c} = 0 \tag{A.11}$$

which accepts the following analytical solution:

$$\hat{c}(\xi) = \frac{-j}{nFD}\xi\mathrm{Q}\left(-\frac{1}{3}, \xi^3\right) \tag{A.12}$$

Here Q is the regularized upper incomplete gamma function, which can be expressed in terms of the upper incomplete gamma function $\mathrm{Q}\left(-\frac{1}{3},\xi^3\right) = \frac{\Gamma\left(-\frac{1}{3},\xi^3\right)}{\Gamma\left(-\frac{1}{3}\right)}$. This function is defined as an indefinite integral as $\Gamma(-1/3,\xi^3) = \int_{\xi^3}^{\infty} t^{-4/3}\mathrm{e}^{-t}dt$, where $\frac{1}{\Gamma\left(-\frac{1}{3}\right)} \approx -0.246$. Solutions

can be seen in Fig. A.4. Undoing the transformations of equations (4) and (A.12) we obtain

$$c(\xi) = c_\infty - \frac{jx}{nFD}\mathrm{Q}\left(-\frac{1}{3}, \xi^3\right) \tag{A.13}$$

from where we find the concentration at the wall:

$$c_\mathrm{w} \approx c_\infty + 0.74\frac{jL_z}{nFD} \tag{A.14}$$

where $\lim_{\xi\to 0}\xi Q\left(-\frac{1}{3}, \xi^3\right) = \frac{-3}{\Gamma(-1/3)} \approx 0.7385$.

The local mass transfer coefficient $k \equiv \frac{D}{c_\infty - c_\mathrm{w}}\left.\frac{\partial c}{\partial x}\right|_\mathrm{w}$, using equations (2) and (A.14), reads

$$k = \frac{\Gamma(-1/3)}{-3}\frac{D}{L_z} \approx 1.354\frac{D}{L_z} \tag{A.15}$$

We introduce a reference concentration c_ref, which may be c_∞ in case it is non-zero, to define a dimensionless concentration profile

$$\bar{c} = \frac{c - c_\infty}{c_\mathrm{ref}} \tag{A.16}$$

Introducing the Damkhöler number

$$\mathrm{Da}_z = -\frac{jL_z}{nFDc_\mathrm{ref}} \tag{A.17}$$

we obtain

$$\bar{c} = \mathrm{Da}_z\xi\mathrm{Q}\left(-\frac{1}{3}, \xi^3\right) \tag{A.18}$$

which can be seen in Fig. A.4. The dimensionless wall concentration then reads:

$$\bar{c}_\mathrm{w} = \frac{3\mathrm{Da}_z}{\Gamma\left(-\frac{1}{3}\right)} \tag{A.19}$$

and the local Sherwood number kz/D:

$$\mathrm{Sh}_z = -\frac{\Gamma\left(-\frac{1}{3}\right)}{3}\frac{z}{L_z} \approx 1.3541\frac{z}{L_z} \tag{A.20}$$

Finally, the 99% boundary layer thickness $\delta_{99\%}$ may be defined as that distance at which the difference with the bulk concentration has decreased to 1% of the concentration difference between the wall and the bulk. Equations (A.13) and (A.14) can be solved for $\frac{c(\xi)-c_\infty}{c_\mathrm{w}-c_\infty} = -1.354\xi\mathrm{Q}\left(-\frac{1}{3}, \xi^3\right) = \xi\frac{\Gamma\left(-\frac{1}{3}, \xi^3\right)}{3} = 0.01$ to give $\xi = 1.31918$ so $\delta_{99\%} \approx 1.32L_z$. Alternatively, we can say that at $x = L_z$ (i.e., $\xi = 1$), the concentration has decreased to approximately $\sim 6.34\%$, which confirms that L_z can be seen as a rough estimate of the mass transfer boundary layer's thickness.

In case of mass transfer of reactants ($j < 0$) a zero wall concentration $c_\mathrm{w} = 0$ is approached at a limiting current $j_\mathrm{lim} = 1.354\frac{nFDc_\infty}{L_z}$. This will happen at the top of the electrode where L_z is the highest.

Comparing equations (A.20) or (A.15) and (A.8) or (A.5) for the Sherwood numbers or mass transfer coefficients using Neumann and Dirichlet boundary conditions, respectively, we obtain

$$\frac{\mathrm{Sh}_{z,\mathrm{D}}}{\mathrm{Sh}_{z,\mathrm{N}}} = \frac{-9}{\Gamma(-1/3)\Gamma(1/3)} = \frac{3\sqrt{3}}{2\pi} \approx 0.827 \tag{A.21}$$

References

[1] J. Lee, A. Alam, C. Park, S. Yoon, H. Ju, Modeling of gas evolution processes in porous electrodes of zero-gap alkaline water electrolysis cells, Fuel 315 (2022) 123273, https://doi.org/10.1016/j.fuel.2022.123273.

[2] D. Le Bideau, P. Mandin, M. Benbouzid, M. Kim, M. Sellier, F. Ganci, R. Inguanta, Eulerian two-fluid model of alkaline water electrolysis for hydrogen production, Energies 13 (2020) 1–14, https://doi.org/10.3390/en13133394.

[3] F. Khalighi, N.G. Deen, Y. Tang, A.W. Vreman, Hydrogen bubble growth in alkaline water electrolysis: an immersed boundary simulation study, Chem. Eng. Sci. 267 (2023), https://doi.org/10.1016/j.ces.2022.118280.

[4] K. Li, Q. Fan, H. Chuai, H. Liu, S. Zhang, X. Ma, Revisiting chlor-alkali electrolyzers: from materials to devices, https://doi.org/10.1007/s12209-021-00285-9, 2021.

[5] K. Hedenstedt, N. Simic, M. Wildlock, E. Ahlberg, Current efficiency of individual electrodes in the sodium chlorate process: a pilot plant study, J. Appl. Electrochem. 47 (2017) 991–1008, https://doi.org/10.1007/s10800-017-1100-3.

[6] A.V. Suzdaltsev, A.Y. Nikolaev, Y.P. Zaikov, Towards the stability of low-temperature aluminum electrolysis, J. Electrochem. Soc. 168 (2021) 046521, https://doi.org/10.1149/1945-7111/abf87f.

[7] M. Ishii, T. Hibiki, Thermofluid Dynamics of Two-Phase Flow, Springer, 2011.

[8] J. Ham, G. Homsy, Hindered settling and hydrodynamic dispersion in quiescent sedimenting suspensions, Int. J. Multiph. Flow 14 (1988) 533–546, https://doi.org/10.1016/0301-9322(88)90056-0.

[9] S. Ostrach, An analysis of laminar free-convection flow and heat transfer about a flat plate parallel to the direction of the generating body force, Technical Report, National Advisory Commitee for Aeronautics, 1953.

[10] E.M. Sparrow, J.L. Gregg, Laminar free convection from a vertical plate with uniform surface heat flux, J. Fluids Eng. 78 (1956) 435–440, https://doi.org/10.1115/1.4013697.

[11] E.M. Sparrow, R. Eichhorn, J.L. Gregg, Combined forced and free convection in a boundary layer flow, Phys. Fluids 2 (1959) 319–328, https://doi.org/10.1063/1.1705928.

[12] T. Chen, H. Tien, B. Armaly, Natural convection on horizontal, inclined, and vertical plates with variable surface temperature or heat flux, Int. J. Heat Mass Transf. 29 (1986) 1465–1478, https://doi.org/10.1016/0017-9310(86)90061-X.

[13] H.T. Lin, W.S. Yu, S.L. Yang, Free convection on an arbitrarily inclined plate with uniform surface heat flux, Wärme- Stoffübertrag. 24 (1989) 183–190, https://doi.org/10.1007/BF01590018.

[14] A.J. Ede, Advances in free convection, Adv. Heat Transf. 4 (1967) 1–64, https://doi.org/10.1016/S0065-2717(08)70272-7.

[15] N. Valle, J.W. Haverkort, Self-similar solution for laminar bubbly flow evolving from a vertical plate, in Prep., http://arxiv.org/abs/2401.13113, arXiv:2401.13113, 2024.

[16] P.L. Chambre, On chemical surface reactions in hydrodynamic flows, Appl. Sci. Res., Sect. A 6 (1956) 97–113, https://doi.org/10.1007/BF03185029.

[17] A. Acrivos, P.L. Chambre, Laminar boundary layer flows with surface reactions, Ind. Eng. Chem. 49 (1957) 1025–1029, https://doi.org/10.1021/ie50570a037.

[18] P.L. Chambré, J.D. Young, On the diffusion of a chemically reactive species in a laminar boundary layer flow, Phys. Fluids 1 (1958) 48–54, https://doi.org/10.1063/1.1724336.

[19] J. Kestin, L. Persen, The transfer of heat across a turbulent boundary layer at very high Prandtl numbers, Int. J. Heat Mass Transf. 5 (1962) 355–371, https://doi.org/10.1016/0017-9310(62)90026-1.

[20] D.E. Rosner, Effects of convective diffusion on the apparent kinetics of zeroth order surface-catalysed chemical reactions, Chem. Eng. Sci. 21 (1966) 223–239, https://doi.org/10.1016/0009-2509(66)85016-9.

[21] L. Donovan, O. Hanna, S. Yerazunis, Similar solutions of turbulent boundary layer heat and mass transfer problems, Chem. Eng. Sci. 22 (1967) 595–610, https://doi.org/10.1016/0009-2509(67)80042-3, https://linkinghub.elsevier.com/retrieve/pii/0009250967800423.

[22] A. Acrivos, On the solution of the convection equation in laminar boundary layer flows, Chem. Eng. Sci. 17 (1962) 457–465, https://doi.org/10.1016/0009-2509(62)85014-3.

[23] A. Acrivos, The asymptotic form of the laminar boundary-layer mass-transfer rate for large interfacial velocities, J. Fluid Mech. 12 (1962) 337–357, https://doi.org/10.1017/S0022112062000257.

[24] E. Lightfoot, Free-convection heat and mass transfer: the limiting case of $\mathrm{Gr}_{AB}/\mathrm{Gr} \to 0$ and $\mathrm{Pr}/\mathrm{Sc} \to 0$, Chem. Eng. Sci. 23 (1968) 931.

[25] J.W. Taunton, E.N. Lightfoot, W.E. Stewart, Simultaneous free-convection heat and mass transfer in laminar boundary layers, Chem. Eng. Sci. 25 (1970) 1927–1937, https://doi.org/10.1016/0009-2509(70)87010-5.

[26] B. Gebhart, L. Pera, The nature of vertical natural convection flows resulting from the combined buoyancy effects of thermal and mass diffusion, Int. J. Heat Mass Transf. 14 (1971) 2025–2050, https://doi.org/10.1016/0017-9310(71)90026-3.

[27] H.-T.T. Lin, C.-M.M. Wu, Combined heat and mass transfer by laminar natural convection from a vertical plate with uniform heat flux and concentration, Heat and Mass Transfer 32 (1997) 293–299, https://doi.org/10.1007/s002310050124.

[28] K.T. Lee, Natural convection heat and mass transfer in partially heated vertical parallel plates, Int. J. Heat Mass Transf. 42 (1999) 4417–4425, https://doi.org/10.1016/S0017-9310(99)00089-7.

[29] R.B. Bird, W.E. Stewart, E. Lightfoot, Transport Phenomena, rev. 2nd ed., Wiley, New York, 2007.

[30] R. Ghez, Mass transport and surface reactions in lévêque's approximation, Int. J. Heat Mass Transf. 21 (1978) 745–750, https://doi.org/10.1016/0017-9310(78)90036-4.

[31] H.H. Hoe, R.R. Farnood, D.W. Kirk, Analytic mathematical model for concentration profile in a parallel plate electrolyzer with variable current density, J. Electrochem. Soc. 164 (2017) E3531–E3538, https://doi.org/10.1149/2.0561711jes.

[32] K. Stephan, H. Vogt, A model for correlating mass transfer data at gas evolving electrodes, Electrochim. Acta 24 (1979) 11–18, https://doi.org/10.1016/0013-4686(79)80033-X.

[33] L. Janssen, Behaviour of and mass transfer at gas-evolving electrodes, Electrochim. Acta 34 (1989) 161–169, https://doi.org/10.1016/0013-4686(89)87081-1.

[34] L.J. Janssen, E. Barendrecht, Mechanism of mass transfer of indicator ions to an oxygen-evolving and a hydrogen-evolving electrode in alkaline solution, Electrochim. Acta 30 (1985) 683–694, https://doi.org/10.1016/0013-4686(85)80112-2.

[35] H. Vogt, The rate of gas evolution of electrodes—I. An estimate of the efficiency of gas evolution from the supersaturation of electrolyte adjacent to a gas-evolving electrode, Electrochim. Acta 29 (1984) 167–173, https://doi.org/10.1016/0013-4686(84)87043-7.

[36] A. Rajora, J.W. Haverkort, An analytical multiphase flow model for parallel plate electrolyzers, Chem. Eng. Sci. 260 (2022) 117823, https://doi.org/10.1016/j.ces.2022.117823.

[37] A.A. Dahlkild, Modelling the two-phase flow and current distribution along a vertical gas-evolving electrode, J. Fluid Mech. 428 (2001) 249–272, https://doi.org/10.1017/S0022112000002639.

[38] J. Schillings, O. Doche, J. Deseure, Modeling of electrochemically generated bubbly flow under buoyancy-driven and forced convection, Int. J. Heat Mass Transf. 85 (2015) 292–299, https://doi.org/10.1016/j.ijheatmasstransfer.2015.01.121.

[39] M.G. Fouad, G.H. Sedahmed, Mass transfer at horizontal gas-evolving electrodes, Electrochim. Acta 18 (1973) 55–58, https://doi.org/10.1016/0013-4686(73)87010-0.

[40] M.G. Fouad, T. Gouda, Natural convection mass transfer at vertical electrodes, Electrochim. Acta 9 (1964) 1071–1076, https://doi.org/10.1016/0013-4686(64)80076-1.